Robust atomic orbital in the cluster magnet LiMoO$_2$

N. Katayama,[1,*] H. Takeda,[2] T. Yamaguchi [©],[3] Y. Yamada,[1] K. Iida [©],[4] M. Takigawa [©],[2] Y. Ohta [©],[3] and H. Sawa[1]

[1]*Department of Applied Physics, Nagoya University, Furo-cho, Chikusa-ku, Nagoya, Aichi 464-8603, Japan*
[2]*Institute for Solid State Physics, University of Tokyo, Kashiwa, Chiba 277-8581, Japan*
[3]*Department of Physics, Chiba University, 1-33 Yayoi-cho, Inage-ku, Chiba 263-8522, Japan*
[4]*Neutron Science and Technology Center, Comprehensive Research Organization for Science
and Society (CROSS), Tokai, Ibaraki 319-1106, Japan*

In this study, we present a rutile-related material, LiMoO$_2$, that becomes a cluster magnet and exhibits a spin singlet formation on a preformed molybdenum dimer upon cooling. Unlike ordinary cluster magnets, the atomic d_{yz} orbital robustly survives despite the formation of molecular orbitals, thereby affecting the magnetic properties of the selected material. Such hybrid cluster magnets with the characters of molecular and atomic orbitals realize multiple independent spins on an isolated cluster, leading to an ideal platform to study the isolated spin dimers physics.

Transition metal compounds with multiple electron degrees of freedom frequently form molecular orbitals in a spin singlet state [1–10]. Examples include trimers of LiVX_2 ($X =$ O, S) [6,8] and dimers of VO$_2$, NbO$_2$, and MoO$_2$ [11–18]. Molecular orbital formation has been attracting considerable attention because it occasionally accompanies a drastic metal-insulator transition [1–4,6] and/or giant entropy changes [5,6,8]. This enables several possible applications in thermochromics [19,20], nonvolatile memory [21], and phase change materials [5,22–25]. Moreover, by arranging additional spins in the molecular orbital, exotic magnetic materials, called cluster magnets, can be obtained [26–35].

LiZn$_2$Mo$_3$O$_8$ is an example of cluster magnets, where inherently formed trimer clusters of molybdenum ions collectively produce a spin $S = 1/2$ moment [26,27]. Due to the frustration effect between trimer clusters arranged in a triangular lattice, an exotic resonating valence bond state emerges at low temperature [26,27]. The hollandite-type K$_2$Mo$_8$O$_{16}$ is another example, comprising molybdenum tetramer clusters with a spin $S = 1/2$. Despite the strong antiferromagnetic interaction with the Weiss temperature of -34 K, the long-range ordering is suppressed to 2 K, with the expectation of the realization of a spin-liquid-like state [28,29].

Rutile and its related compounds are an ideal playground to explore novel cluster magnets because dimers frequently appear there and lithium intercalation is available to tune the electronic states. Lithium intercalation supplies electrons to the host structure, resulting in an additional spin to the preformed dimers, possibly leading to the development of novel cluster magnets. Here, we focus our attention on a d^2 compound, MoO$_2$, and its lithium intercalated derivatives. In the parent MoO$_2$, preformed dimers are formed, indicating that molecular orbitals are realized [17,18]. The preformed

dimers are formed by a σ bonding, while π orbitals are strongly coupled with oxygen p orbitals, resulting in a high metallic conductivity [17,36]. Note that the schematics of atomic orbitals composing σ and π orbitals are shown in Figs. 4(a) and 4(b). Although details of the structural and physical properties of lithium intercalation compounds are yet to be clarified, the previous magnetic susceptibility measurements have shown that an anomalous temperature dependence appears in LiMoO$_2$ [37], as shown in Fig. 3(a), with the expectation of an unusual magnetic property of a cluster magnet.

Here, we first show that Li$_{0.5}$MoO$_2$ and LiMoO$_2$ display different patterns of preformed molybdenum dimers. While Li$_{0.5}$MoO$_2$ is a paramagnetic metal, LiMoO$_2$ becomes a Mott insulator with two localized electrons on a molybdenum preformed dimer. Based on our structural and theoretical studies, we conclude that the molybdenum preformed dimers comprise the multiple bonding of σ and π bonds, while the δ bond is not formed, thereby resulting in the localized d electron in original d_{yz} orbitals, as shown in Fig. 4(e). On cooling, the two spins on a molybdenum dimer form a spin singlet ground state. Therefore, LiMoO$_2$ is an unusual type of magnetic cluster where the original d_{yz} orbitals robustly survive on preformed molybdenum dimers.

Powder samples of LiMoO$_2$ were prepared by a soft-chemical method. Commercial MoO$_2$ powder samples were immersed on 0.2 M n-BuLi hexane solution for 2 days to attain the maximum Li content. By decreasing the n-BuLi concentration, we successfully obtained Li$_{0.5}$MoO$_2$. The Li content of Li$_{0.5}$MoO$_2$ and LiMoO$_2$ was estimated to be approximately 0.5 and 1.0, respectively, by referring to the lattice parameters presented in a previous study [38]. For LiMoO$_2$, Li content was also estimated to be 0.98(2) from the Rietveld analysis of synchrotron x-ray diffraction experiments. Details of other experimental methods are summarized in the Supplemental Material [39].

*katayama.naoyuki@b.mbox.nagoya-u.ac.jp
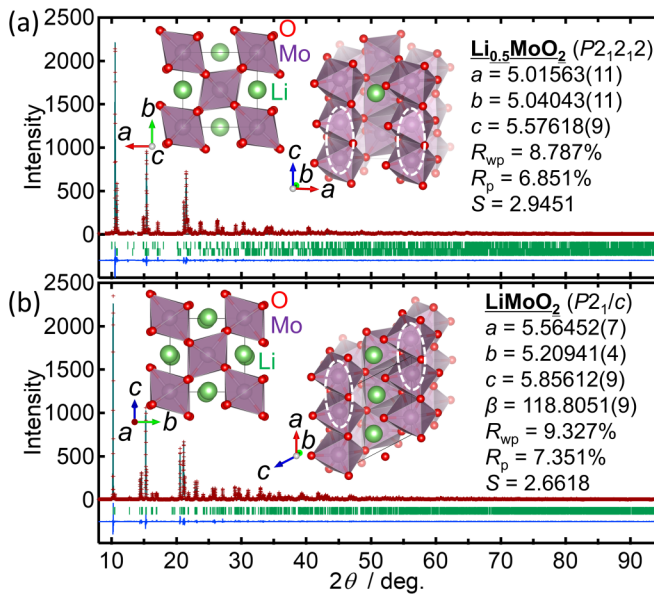
FIG. 1. Rietveld analysis results of (a) $Li_{0.5}MoO_2$ and (b) $LiMoO_2$, obtained at room temperature. In $Li_{0.5}MoO_2$ data, ~27% of $Li_{0.2}MoO_2$ with a space group $P2_1/c$ was identified as an impurity. Insets indicate the crystal structures. Dotted ovals indicate the preformed molybdenum dimers. Note that similar dimer patterns are realized in $LiMoO_2$ and MoO_2.

FIG. 2. (a) Average of the six Mo-O distances constituting the MoO_6 octahedron. (b) Temperature dependence of x-ray diffraction patterns of $LiMoO_2$. (c) X-ray appearance near-edge structure spectra for MoO_2, $Li_{0.5}MoO_2$, and $LiMoO_2$. (d) Mo-Mo distances consisting of preformed dimers.

Figures 1(a) and 1(b) show the Rietveld analysis of $Li_{0.5}MoO_2$ and $LiMoO_2$. The Rietveld analysis of MoO_2 is shown in the Supplemental Material [39]. While MoO_2 and $LiMoO_2$ were successfully refined by assuming the same monoclinic space group $P2_1/c$, an orthorhombic space group $P2_12_12$ was used to refine $Li_{0.5}MoO_2$. While the refined crystal structures of MoO_2 and $LiMoO_2$ were consistent with those reported before [40], the crystal structure of $Li_{0.5}MoO_2$ was identified in this study. Although the emergence of preformed molybdenum dimers was identified in all the materials measured, the dimer arrangements of $Li_{0.5}MoO_2$ were different from those of MoO_2 and $LiMoO_2$. This indicates that the dimer arrangement was changed twice during the lithium intercalation. In $Li_{0.5}MoO_2$, the molybdenum dimers are located away from the intercalated lithium ions probably due to the Coulomb repulsion between periodically inserted lithium ions and molybdenum dimers. After multiple structural phase transitions, similar dimer arrangements were restored in $LiMoO_2$ with MoO_2. The refined structural parameters are presented in the Supplemental Material [39].

While the preformed molybdenum dimers commonly appear in these compounds, considerable differences exist in the local structures. Figure 2(a) shows the averaged Mo-O distances obtained from the six Mo-O bonds constituting the MoO_6 octahedron. Note that the averaged Mo-O distance is kept almost constant up to the decomposition temperature of ~550 K for $LiMoO_2$, as shown in Fig. 2(b). Compared with MoO_2 and $Li_{0.5}MoO_2$, the averaged Mo-O distance is ~0.1 Å longer for $LiMoO_2$. Considering lithium intercalation inevitably changes the formal valence of molybdenum from the 4+ to the 3+ side, one may consider that the increase in the ionic radius of molybdenum ions is responsible for the elongation. Note that the change in the formal valence of molybdenum caused by the lithium intercalation was confirmed from the molybdenum K-edge extended x-ray-absorption fine-structure (EXAFS) experiment, as shown in Fig. 2(c). The edge energy is shifted to the lower energy side in the order of MoO_2-$Li_{0.5}MoO_2$-$LiMoO_2$, indicating that the formal valence of molybdenum changes from the 4+ to the 3+ side via lithium intercalation. However, according to Shannon ionic radii [41], the ionic radii of octahedrally coordinated Mo^{3+} and Mo^{4+} are 0.69 and 0.65 Å, respectively. The difference, 0.04 Å, is very small to explain why the change of the averaged Mo-O distance reaches ~0.1 Å. Therefore, we expect that the $Mo4d$-$O2p$ orbital hybridization becomes weaker in $LiMoO_2$ compared with MoO_2 and $Li_{0.5}MoO_2$. Conversely, the Mo-Mo distance of preformed dimers becomes 0.03 Å shorter in $LiMoO_2$ compared with MoO_2, as shown in Fig. 2(d), indicating that the molybdenum dimers are enhanced in $LiMoO_2$ compared with MoO_2.
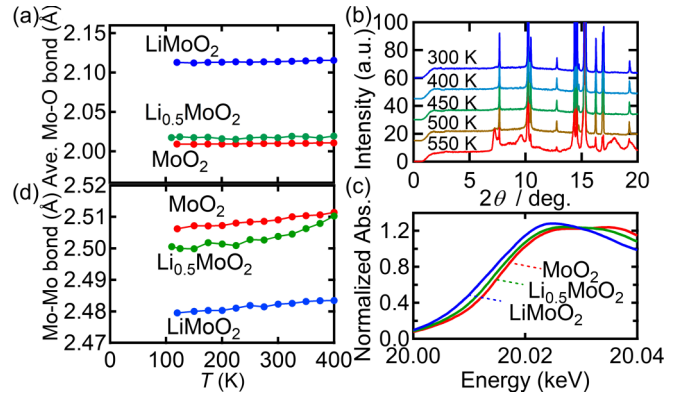
Next, we revisit the physical properties of these samples. These results are basically consistent with the previous data [37,42]. An almost temperature-independent Pauli paramagnetism was observed for MoO_2 and $Li_{0.5}MoO_2$ from the magnetic susceptibility experiment [37]. Correspondingly, the low temperature sintered samples of MoO_2 and $Li_{0.5}MoO_2$ show a metallic conductivity down to the lowest temperature measured [42]. However, a strong temperature dependence appears in $LiMoO_2$, as shown in Fig. 3(a). The observed behaviors are qualitatively consistent with those previously reported [37], although the origin of the strong temperature dependence on $LiMoO_2$ is yet to be clarified. When the band structure near the Fermi surface has a characteristic shape, temperature-dependent behavior occasionally appears even in a Pauli paramagnetic metal. However, our low temperature sintered sample of $LiMoO_2$ showed no electrical conductivity at room temperature [37]. This suggests that $LiMoO_2$ is essentially an insulator with a large charge gap and the temperature dependence of the magnetic susceptibility is not derived from the Pauli paramagnetism.

Because $LiMoO_2$ is inherently an insulator, we can expect that the antiferromagnetic or spin singlet state should be
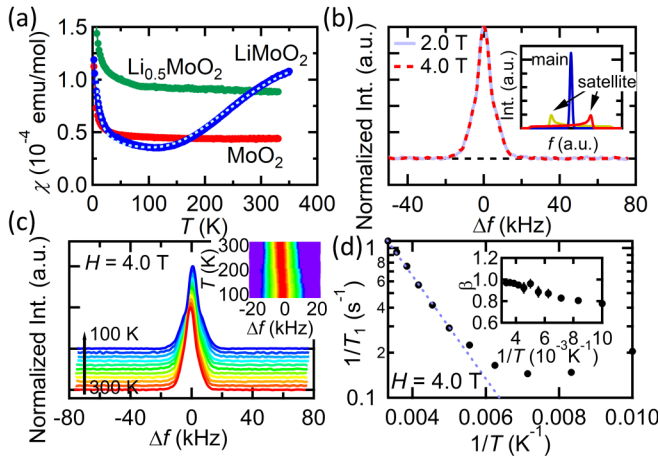
FIG. 3. (a) Magnetic susceptibility for MoO_2, $Li_{0.5}MoO_2$, and $LiMoO_2$. $H = 1$ T was applied for collecting the data. For $LiMoO_2$, the data was fitted by the white dotted line using the equation for isolated dimers [43]. (b) ^{7}Li-NMR spectra obtained at 200 K for magnetic fields of 2.0 and 4.0 T for $LiMoO_2$. Δf is defined as the frequency shift measured from the reference frequency, $\Delta f = f - \gamma H$. Inset shows the simulated pattern of typical powder patterns for $-3/2 \leftrightarrow -1/2$ (red), $3/2 \leftrightarrow 1/2$ (yellow), and $-1/2 \leftrightarrow 1/2$ (blue) when $I = 3/2$. (c) Temperature dependencies on ^{7}Li-NMR spectra for $LiMoO_2$. Inset shows the contour map of the intensity at various temperatures. (d) Spin-lattice relaxation rate $(1/T_1)$ and the Arrhenius plot with the function of $1/T_1 = a \exp(-\Delta/T)$ for $LiMoO_2$. The inset shows the temperature dependence of the stretch exponent, β.

realized. To identify the magnetic ground state, ^{7}Li-NMR measurement of $LiMoO_2$ was performed. The NMR spectrum at 200 K displayed in Fig. 3(b) shows a relatively sharp central peak on top of a slightly broader line. The latter corresponds to the quadrupole satellite ($\pm 3/2 \leftrightarrow \pm 1/2$) transitions, although the line shape is quite different from the simulated typical powder pattern shown in the inset. This is because the quadrupole shift is very small, comparable with the width of the central line which is likely to be determined by field-independent nuclear dipole-dipole interactions. As shown in Fig. 3(c) and its inset, the linewidth of the main peak is unchanged when the temperature is reduced. These results show that the ground state is not antiferromagnetic. The linewidth of the satellite line slightly broadens with decreasing temperature, which may be due to reduced mobility of lithium ions. The spin-lattice relaxation rate, $1/T_1$, follows an activation law as shown in Fig. 3(d), indicating the emergence of a spin gap at low temperature. The size of the spin gap was estimated to be approximately 800 K from the Arrhenius plot. The $1/T_1$ deviates from the activation law below ∼180 K, accompanied by a moderate decrease of stretch exponent β from unity. This is ascribed to the appearance of some inhomogeneous spin-relaxation process such as the relaxation via impurity spins or lithium motion.

As presented above, our experimental findings clearly indicate that $LiMoO_2$ is essentially an insulator with a spin gap. Next, we discuss the origin of the spin gap from the structural aspects. Compared with MoO_2, the intradimer distance becomes shorter in $LiMoO_2$. This indicates that the
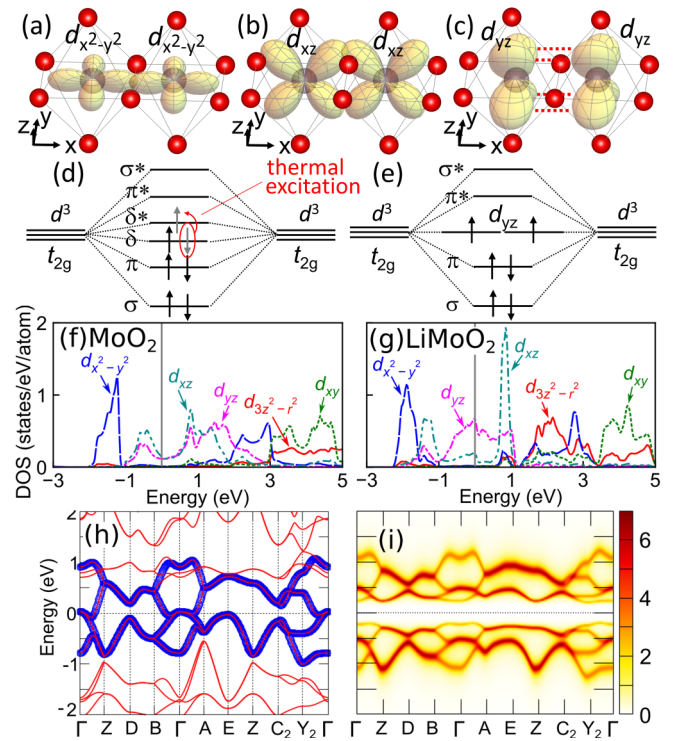
FIG. 4. The electronic structures of $LiMoO_2$ and MoO_2. (a)–(c) Schematics of the atomic orbitals composed of (a) σ, (b) π, and (c) δ bonds. (d), (e) Schematics of the energy levels of the molecular orbitals of a molybdenum dimer where the gap opens between the δ and δ^* orbitals (d) but two nearly degenerate levels appear when the δ bonding is negligible (e). (f), (g) Calculated PDOSs for MoO_2 (f) and $LiMoO_2$ (g). (h) Calculated band dispersions (red lines) compared with the tight-binding band dispersions obtained using four d_{yz} MLWFs (blue lines). GGA ($U = 0$ eV) is used for the calculations in (f)–(h). (i) Intensity plot of the single-particle spectral function calculated by the DMFT where we assume $U = 1$ eV.

preformed dimer is enhanced in $LiMoO_2$. A possible scenario is that hybridization of the π molecular orbital and O$2p$ orbital become weak in $LiMoO_2$, while the π bond strengthens the molybdenum preformed dimer. That is, the multiple bonds comprising σ and π bonds are realized in $LiMoO_2$, as shown in Figs. 4(a) and 4(b). This bonding state is distinctly different from that in MoO_2, where the π molecular orbital is strongly hybridized with the O$2p$ orbital, resulting in strong electronic conductivity. Compared with MoO_2, the averaged Mo-O distance is apparently longer in $LiMoO_2$, suggesting weak hybridization of the π molecular orbital and O$2p$ orbital.

$LiMoO_2$ has d^3 electrons, and two of the three electrons contribute to the formation of σ and π bonds. Therefore, the remaining third electron should produce the spin gap. Two possible scenarios exist on the role of the third electron.

The first is that the third electron forms a δ bond, as shown in Fig. 4(c), resulting in $LiMoO_2$ becoming a band insulator with a narrow gap between the δ and δ^* orbitals, as shown in Fig. 4(d). When the gap between δ and δ^* orbitals is narrow, electrons in δ orbitals can be thermally excited into δ^* orbitals. The increasing numbers of thermally excited isolated spins should produce strong temperature-dependent magnetic susceptibility on heating. However, this scenario does not

seem to happen. From the ^{7}Li-NMR experiment, a spin gap, relating to the singlet-triplet excitation, was estimated to be approximately 800 K. If LiMoO$_2$ is a narrow-gap band insulator with a gap of approximately 800 K, the charge gap should be consistent with the spin gap. Therefore, many carriers should be thermally excited across the charge gap even at room temperature, leading to a high electrical conductivity. However, this critically contradicts our results. The charge gap should be considerably larger than the spin gap.

The second is that the δ bonding is absent in LiMoO$_2$, while the third electron locates at the robustly surviving d_{yz} orbital, as shown in Fig. 4(e). In this scenario, LiMoO$_2$ is inherently a Mott insulator with the third electron localized at each molybdenum site with a spin $S = 1/2$. On cooling, a spin singlet is formed between the neighboring third electrons localized on the preformed dimers. We can intuitively understand that this can happen because the overlap between adjacent d_{yz} orbitals should be very small, as shown in Fig. 4(c), leading to the destabilization of δ-bond formation. If the d_{yz} orbitals robustly survive and form a dimer between localized spins, it is expected that the magnetic susceptibility data can be fitted using the equation of the isolated dimers. This fitting was successfully done using the following equation [43]:

$$\chi = \frac{Ng^2\mu^2}{k_BT}\frac{1}{3+e^{J/k_BT}} + \frac{C}{T} + B,$$

where the second and third terms indicate the Curie impurity and temperature-independent Van Vleck terms with $\chi_{VV} = 2.98(3) \times 10^{-5}$ emu/mol. The estimated Curie constant of $C = 4.93(8) \times 10^{-4}$ emu/mol Mo K implies the existence of a tiny amount of paramagnetic impurities of less than 1% if we assume a spin-1/2 moment. The effective magnetic moment is estimated to be $g\mu = 0.60(2)\mu_B$, which is apparently smaller than the expected value. This possibly appears due to the weak hybridization between the robust Mo 4d_{yz} orbital and surrounding O 2p orbitals, and/or spatially extended 4d orbitals compared to 3d orbitals. The fitting gives the great fit with $J/k_B \sim 894$ K, comparable to the estimated spin gap of $\sim$800 K from NMR experiment. The difference may be attributed to the narrow temperature window for fitting. This result supports that the present material can be treated as an isolated spin dimer model on a preformed dimer. The estimated spin gap of approximately 800 K seems to be unusually large for a spin $S = 1/2$ system, possibly because the shortening of the Mo-Mo distance caused by the preformed multiple bonds strengthens the exchange interaction between spins. In this scenario, the charge gap is expected to be considerably larger than the spin gap because LiMoO$_2$ is essentially a Mott insulator over the entire temperature range.

Second, we elaborate on the electronic states of the relevant materials from a theoretical perspective. Here, we applied the density functional theory (DFT) based on electronic structure calculations and the dynamical mean-field theory (DMFT) calculations [44]. For the DFT calculations, we used the WIEN2K code [45] based on the full-potential linearized augmented-plane-wave method. We present calculated results obtained in the generalized gradient approximation (GGA) for electron correlations with the exchange-correlation potential of Ref. [46]. To improve the description of electron

correlations in the Mo 4d orbitals, we used a rotationally invariant version of the GGA $+ U$ method with double-counting correction in the fully localized limit [47,48]. In the self-consistent calculations, we typically use $\sim$12 $\times$ 12 $\times$ 12 $\mathbf{k}$ points in the full Brillouin zone. Muffin-tin radii (R_{MT}) of 1.54 (Li), 1.90 (Mo), and 1.74 (O) bohrs are used, and the plane-wave cutoff of $K_{\max} = 7.00/R_{\mathrm{MT}}$ is assumed.

The calculated results for the densities of states (DOSs) are shown in Fig. 4(f) for MoO$_2$ and in Fig. 4(g) for LiMoO$_2$. For MoO$_2$, we find that the partial DOS (PDOS) projected onto each 4d orbital of a Mo ion corresponds perfectly with the previous work [36], where we note that, reflective of the strong σ-bonding nature, the bonding (antibonding) state of the $d_{x^2-y^2}$ orbitals is located $\sim$2 eV below (above) the Fermi level and the states from the d_{xz} and d_{yz} orbitals are located around the Fermi level, resulting in the metallic nature of the material. For LiMoO$_2$, we found that the bonding (antibonding) states of both the $d_{x^2-y^2}$ and d_{xz} orbitals are located considerably below (above) the Fermi level, thereby allowing the assumption that the low-energy electronic properties are well described only by the d_{yz} orbitals. Therefore, the standard DFT calculations predict that LiMoO$_2$ should be a metal; however, this contradicts the result of the experiment.

As shown in Figs. 4(d) and 4(e), the insulating behavior of LiMoO$_2$ can be explained by the band-insulator and Mott-insulator scenarios. In principle, the former may be justified by the DFT band-structure calculations. This is particularly the case when we introduce the on-site orbital potential U in the GGA $+ U$ scheme; however, we find that the band gap opens only if an unrealistically large value of $U \gtrsim 10$ eV is introduced. Therefore, we may conclude that the band-insulator scenario is highly unlikely.

Because the Mott-insulator state cannot be described by the DFT calculations, we apply the DMFT calculations [44], using the DCore library [49] based on TRIQS [50,51]. The Hubbard-I approximation is used for the impurity solver, which is known to provide successful results in well-localized systems [52–54]. For the calculations, we first create a tight-binding band structure using four maximally localized Wannier functions (MLWFs) [55,56], that corresponds well with the DFT band structure, as shown in Fig. 4(h), indicating that the low-energy electronic structure of this system is well described by the four d_{yz} orbitals of Mo ions. The calculated result for the single-particle spectra at $U = 1$ eV and $T \sim 300$ K in the DMFT is shown in Fig. 4(i) where we find that the band gap of a size $\sim$0.5 eV is clearly visible, indicating that the system is a Mott insulator. The gap size can be controlled by adjusting the value of U. We note that using an elaborative solver such as a continuous-time quantum Monte Carlo solver, or a self-consistent DFT $+$ DMFT calculation, can facilitate more quantitative discussions on this material; however, this is beyond the scope of this Rapid Communication.

Finally, let us verify the experimentally estimated spin gap from a theoretical point of view. Based on the tight-binding calculation results, we can estimate the hopping integral t between nearest-neighbor Mo ions to be $\sim$0.2 eV. Assuming that the experimentally obtained spin gap of 800–900 K, corresponding to 0.069–0.078 eV, is consistent with the exchange interaction J based on the two-body model, we can estimate the on-site Coulomb interaction $U \sim 2.06$–2.32 eV

through the function of $J \sim 4t^2/U$. This result is quite valid considering that $LiMoO_2$ is a $4d$-electron system.

Thus, we can conclude that $LiMoO_2$ is a hybrid cluster magnet with the characters of molecular and atomic orbitals. Although robust atomic orbital is a unique feature of $LiMoO_2$ which cannot be found in ordinary cluster magnets, we can expect such electronic states can be realized on other cluster magnets as well when the outermost molecular orbital is unstable. This realizes an unusual situation in which one cluster possesses multiple independent spins, providing an ideal platform to study isolated spin dimers physics.

[1] S. A. J. Kimber, I. I. Mazin, J. Shen, H. O. Jeschke, S. V. Streltsov, D. N. Argyriou, R. Valentí, and D. I. Khomskii, Phys. Rev. B **89**, 081408(R) (2014).

[2] P. G. Radaelli, Y. Horibe, M. J. Gutmann, H. Ishibashi, C. H. Chen, R. M. Ibberson, Y. Koyama, Y. S. Hor, V. Kiryukhin, and S. W. Cheong, Nature (London) **416**, 155 (2002).

[3] Y. Okamoto, S. Niitaka, M. Uchida, T. Waki, M. Takigawa, Y. Nakatsu, A. Sekiyama, S. Suga, R. Arita, and H. Takagi, Phys. Rev. Lett. **101**, 086404 (2008).

[4] M. Schmidt, W. Ratcliff, P. G. Radaelli, K. Refson, N. M. Harrison, and S. W. Cheong, Phys. Rev. Lett. **92**, 056402 (2004).

[5] N. Katayama, S. Tamura, T. Yamaguchi, K. Sugimoto, K. Iida, T. Matsukawa, A. Hoshikawa, T. Ishigaki, S. Kobayashi, Y. Ohta, and H. Sawa, Phys. Rev. B **98**, 081104(R) (2018).

[6] N. Katayama, M. Uchida, D. Hashizume, S. Niitaka, J. Matsuno, D. Matsumura, Y. Nishihata, J. Mizuki, N. Takeshita, A. Gauzzi, M. Nohara, and H. Takagi, Phys. Rev. Lett. **103**, 146405 (2009).

[7] Y. Horibe, M. Shingu, K. Kurushima, H. Ishibashi, N. Ikeda, K. Kato, Y. Motome, N. Furukawa, S. Mori, and T. Katsufuji, Phys. Rev. Lett. **96**, 086406 (2006).

[8] K. Kojima, N. Katayama, S. Tamura, M. Shiomi, and H. Sawa, Phys. Rev. B **100**, 235120 (2019).

[9] Y. Okamoto, H. Amano, N. Katayama, H. Sawa, K. Niki, R. Mitoka, H. Harima, T. Hasegawa, N. Ogita, Y. Tanaka, M. Takigawa, Y. Yokoyama, K. Takehana, Y. Imanaka, Y. Nakamura, H. Kishida, and K. Takenaka, Nat. Commun. **11**, 3144 (2020).

[10] A. J. Browne, S. A. J. Kimber, and J. P. Attfield, Phys. Rev. Mater. **1**, 052003(R) (2017).

[11] W. Rüdorff, G. Walter, and J. Stadler, Z. Anorg. Allg. Chem. **297**, 1 (1958).

[12] F. J. Morin, Phys. Rev. Lett. **3**, 34 (1959).

[13] V. Eyert, Ann. Phys. **11**, 650 (2002).

[14] Y. Bando, K. Nagasawa, Y. Kato, and T. Takada, Jpn. J. Appl. Phys. **8**, 633 (1969).

[15] R. F. Janninck and D. H. Whitmore, J. Phys. Chem. Solids **27**, 1183 (1966).

[16] V. Eyert, Europhys. Lett. **58**, 851 (2002).

[17] Z. Hiroi, Prog. Solid State Chem. **43**, 47 (2015).

[18] A. A. Bolzan, B. J. Kennedy, and C. J. Howard, Aust. J. Chem. **48**, 1473 (1995).

[19] H. Jerominek, F. Picard, and D. Vincent, Opt. Eng. **32**, 2092 (1993).

[20] A. Cavalleri, C. Toth, C. W. Siders, J. A. Squier, F. Raksi, P. Forget, and J. C. Kieffer, Phys. Rev. Lett. **87**, 237401 (2001).

[21] M. Nakano, K. Shibuya, D. Okuyama, T. Hatano, S. Ono, M. Kawasaki, Y. Iwasa, and Y. Tokura, Nature (London) **487**, 459 (2012).

[22] M. M. Farid, A. M. Khudhair, S. A. K. Razack, and S. Al-Hallaj, Energy Convers. Manage. **45**, 1597 (2004).

[23] A. Sharma, V. V. Tyagi, C. R. Chen, and D. Buddhi, Renewable Sustainable Energy Rev. **13**, 318 (2009).

[24] H. Takagi, M. Miyano, and S. Niitaka, Heat storage material, Japanese Patent Application No. JP 2010-163510A (14 January 2009).

[25] S. Niitaka, H. Takagi, and K. Kohno, Heat storage material, U.S. Patent Application No. US9884983B2 (15 April 2014).

[26] J. P. Sheckelton, J. R. Neilson, D. G. Soltan, and T. M. McQueen, Nat. Mater. **11**, 493 (2012).

[27] M. Mourigal, W. T. Fuhrman, J. P. Sheckelton, A. Wartelle, J. A. Rodriguez-Rivera, D. L. Abernathy, T. M. McQueen, and C. L. Broholm, Phys. Rev. Lett. **112**, 027202 (2014).

[28] T. Ozawa, I. Suzuki, and H. Sato, J. Phys. Soc. Jpn. **75**, 014802 (2006).

[29] T. Toriyama, M. Watanabe, T. Konishi, and Y. Ohta, Phys. Rev. B **88**, 235116 (2013).

[30] M. Marezio, D. McWhan, P. Dernier, and J. Remeika, Phys. Rev. Lett. **28**, 1390 (1972).

[31] C. A. Bridges and J. E. Greedan, J. Solid State Chem. **177**, 1098 (2004).

[32] T. Kajita, T. Kanzaki, T. Suzuki, J. E. Kim, K. Kato, M. Takata, and T. Katsufuji, Phys. Rev. B **81**, 060405(R) (2010).

[33] K. Iida, H. Yoshida, H. Okabe, N. Katayama, Y. Ishii, A. Koda, Y. Inamura, N. Murai, M. Ishikado, R. Kadono, and R. Kajimoto, Sci. Rep. **9**, 1829 (2019).

[34] K. T. Law and P. A. Lee, Proc. Natl. Acad. Sci. USA **114**, 6996 (2017).

[35] M. Kratochvilova, A. D. Hillier, A. R. Wildes, L. Wang, S. W. Cheong, and J. G. Park, npj Quantum Mater. **2**, 42 (2017).

[36] J. Moosburger-Will, J. Kündel, M. Klemm, S. Horn, P. Hofmann, U. Schwingenschlögl, and V. Eyert, Phys. Rev. B **79**, 115113 (2009).

[37] F. J. DiSalvo, D. W. Murphy, and J. V. Waszczak, Synth. Met. **1**, 29 (1979).

[38] J. R. Dahn and W. R. McKinnon, Solid State Ionics **23**, 1 (1987).

[39] See Supplemental Material at http://link.aps.org/supplemental/10.1103/PhysRevB.102.081106 for experimental details and structural aspects.

[40] D. E. Cox, R. J. Cava, D. B. McWhan, and D. W. Murphy, J. Phys. Chem. Solids **43**, 657 (1982).

[41] R. D. Shannon, Acta Crystallogr., Sect. A: Found. Adv. **32**, 751 (1976).

[42] D. B. Bogers, R. D. Shannon, A. W. Sleight, and J. L. Gillson, Inorg. Chem. **8**, 841 (1969).

[43] B. Bleaney and K. D. Bowers, Proc. R. Soc. London, Ser. A **214**, 451 (1952).

[44] K. Haule, C. H. Yee, and K. Kim, Phys. Rev. B **81**, 195107 (2010).

[45] P. Blaha, K. Schwarz, G. K. H. Madsen, D. Kvasnicka, and J. Luitz, *WIEN2k, An Augmented Plane Wave Plus Local Orbitals Program for Calculating Crystal Properties* (Technische Universitat Wien, Austria, 2001).

[46] J. P. Perdew, K. Burke, and M. Ernzerhof, Phys. Rev. Lett. **77**, 3865 (1996).

[47] V. I. Anisimov, I. V. Solovyev, M. A. Korotin, M. T. Czyżyk, and G. A. Sawatzky, Phys. Rev. B **48**, 16929 (1993).

[48] A. I. Liechtenstein, V. I. Anisimov, and J. Zaanen, Phys. Rev. B **52**, R5467 (1995).

[49] H. Shinaoka, J. Otsuki, K. Yoshimi, M. Kawamura, N. Takemori, and Y. Motoyama, DCore library, https://issp-center-dev.github.io/DCore/.

[50] O. Parcollet, M. Ferrero, T. Ayral, H. Hafermann, I. Krivenko, L. Messio, and P. Seth, Comput. Phys. Commun. **196**, 398 (2015).

[51] M. Aichhorn, L. V. Pourovskii, P. Seth, V. Vildosola, M. Zingl, O. E. Peil, X. Deng, J. Mravlje, G. J. Kraberger, C. Martins, M. Ferrero, and O. Parcollet, Comput. Phys. Commun. **204**, 200 (2016).

[52] L. V. Pourovskii, B. Amadon, S. Biermann, and A. Georges, Phys. Rev. B **76**, 235101 (2007).

[53] B. Amadon, J. Phys.: Condens. Matter **24**, 075604 (2012).

[54] A. B. Shick, J. Kolorenč, A. I. Lichtenstein, and L. Havela, Phys. Rev. B **80**, 085106 (2009).

[55] A. A. Mostofi, J. R. Yates, Y. S. Lee, I. Souza, D. Vanderbilt, and N. Marzari, Comput. Phys. Commun. **178**, 685 (2008).

[56] J. Kuneš, R. Arita, P. Wissgott, A. Toschi, H. Ikeda, and K. Held, Comput. Phys. Commun. **181**, 1888 (2010).